How to cite: *Angew. Chem. Int. Ed.* **2024**, *63*, e202407859
doi.org/10.1002/anie.202407859

Single Atom Catalysis | Hot Paper

Development of Iron-Based Single Atom Materials for General and Efficient Synthesis of Amines

Zhuang Ma, Chakreshwara Kuloor, Carsten Kreyenschulte, Stephan Bartling, Ondrej Malina, Michael Haumann, Prashanth W. Menezes, Radek Zbořil, Matthias Beller,* and Rajenahally V. Jagadeesh**

Abstract: Earth abundant metal-based heterogeneous catalysts with highly active and at the same time stable isolated metal sites constitute a key factor for the advancement of sustainable and cost-effective chemical synthesis. In particular, the development of more practical, and durable iron-based materials is of central interest for organic synthesis, especially for the preparation of chemical products related to life science applications. Here, we report the preparation of Fe-single atom catalysts (Fe-SACs) entrapped in N-doped mesoporous carbon support with unprecedented potential in the preparation of different kinds of amines, which represent privileged class of organic compounds and find increasing application in daily life. The optimal Fe-SACs allow for the reductive amination of a broad range of aldehydes and ketones with ammonia and amines to produce diverse primary, secondary, and tertiary amines including N-methylated products as well as drugs, agrochemicals, and other biomolecules (amino acid esters and amides) utilizing green hydrogen.

Introduction

The development of new materials with improved chemical and physical properties is a prerequisite to achieve a sustainable and circular economy in the next two decades.[1–3] In this respect, the preparation of such materials using abundant and inexpensive feedstocks is crucial. Apart from basic carbon- and silicon-based materials, many daily life products require the use of specific rare-earth or precious metals.[4–5] As an example, catalysis in both academic research laboratories and industry relies to a significant extent on noble metals allowing the production of all kinds of bulk and fine chemicals including many life science molecules.[6–8] Indeed, 80–90 % of all processes in today's chemical industry as well as state-of-the-art organic synthesis on catalysis.[8–10] Among these, around 80 % of catalysts used are based on heterogeneous materials.[8–12] As a result, the global market for catalysts in 2023 is valued at USD 39.36 billion and is projected to grow at a Compound Annual Growth Rate (CAGR) of 5 % in the forecast period of 2024–2032.[13]

Clearly, new catalytic materials are the basis for the further advancement of chemistry as a basic science and industry, influencing many other science fields such as biology, medicine, material science, and energy technologies. Notably, contemporary synthesis of complex and functionalized organic molecules in industry still generates a major extent of waste. In fact, the EU fine chemical and pharmaceutical industries have a higher CO_2 footprint than the automotive sector.[14–15] To be consistent with the UN sustainability goals[16] and to solve these problems see above, upcoming catalytic systems should be highly active and selective as well as applicable to a wide variety of substrates including multi-functionalized and sensitive ones. Ideally, they should be based on earth's abundant metals instead of precious ones.[17–21]

[*] Dr. Z. Ma, C. Kuloor, Dr. C. Kreyenschulte, Dr. S. Bartling, Prof. Dr. M. Beller, Prof. Dr. R. V. Jagadeesh
Leibniz-Institut für Katalyse e.V., Albert-Einstein-Str. 29a, Rostock, D-18059, Germany
E-mail: matthias.beller@catalysis.de
jagadeesh.rajenahally@catalysis.de

Dr. O. Malina, Prof. Dr. R. Zbořil, Prof. Dr. R. V. Jagadeesh
Nanotechnology Centre, Centre for Energy and Environmental Technologies, VŠB–Technical University of Ostrava, Ostrava-Poruba, Czech Republic
E-mail: radek.zboril@upol.cz

Dr. O. Malina, Prof. Dr. R. Zbořil
Regional Centre of Advanced Technologies and Materials, Palacky University Olomouc, Olomouc, Czech Republic

Dr. M. Haumann
Physics Department, Freie Universität Berlin, Berlin, Germany

Dr. P. W. Menezes
Helmholtz-Zentrum Berlin für Materialien und Energie, Albert-Einstein-Str. 15, 12489 Berlin, Germany

Dr. P. W. Menezes
Department of Chemistry, Technical University of Berlin, Berlin, Germany

In particular, iron-based systems are preferable due to the inherited advantages of availability, price and their environmentally benign nature.[22–25] Although such materials are well-established to produce bulk chemicals, e.g. ammonia[26–27] and FT-olefins[28–29] their design for advanced organic synthesis is still challenging. In the last decade, the introduction of so-called single atoms catalysts (SACs)[25,30–35] with isolated metal sites has evolved as a strategy to improve the activity of Fe-based heterogeneous materials.[25,36–39] However, the creation of stable isolated metal atoms is a difficult task, due to aggregation and coarsening effects. To avoid these problems, several research groups[36–39] including us[25,39–40] proposed the synthesis of microenvironments with stabilizing Fe–N interactions. To create such highly dispersed metal sites, the use of suitable metal precursors and preparation methodologies are important. As an example, the immobilization of nitrogen-ligated iron complexes on various supports and subsequent pyrolysis has been proven to be a promising technology to create both Fe-NPs[41] and Fe-SACs.[25,36–40]

Based on our longstanding interest in heterogeneous catalysis, here we report the preparation of Fe-based single atoms as highly active and selective catalysts for the industrially relevant reductive amination of carbonyl compounds with ammonia or amines in the presence of molecular hydrogen to prepare benzylic, heterocyclic, and aliphatic primary, secondary and tertiary amines including N-methylated amines. The resulting products represent valuable compounds for the chemical, pharmaceutical, and agrochemical industries.[42–49] In fact, amine-based fine and bulk chemicals are prepared to a significant extent via catalytic reductive aminations, which also make use of easily available carbonyl compounds, ammonia (or other primary or secondary amines) and hydrogen.[44–50] However, to the best of our knowledge no iron-based material is known for the synthesis of different kinds of amines including drugs, agrochemicals, and other biomolecules.

It should be noted that, compared to secondary or tertiary amines, the selective synthesis of primary amines by reductive aminations is challenging. The reaction of carbonyl compounds with ammonia and molecular hydrogen is often non-selective and side reactions such as over hydrogenation to corresponding alcohols and N-arylations likely occur.[46,50] In order to prepare primary amines in a highly selective manner by avoiding these side reactions, the catalyst should be highly active and selective for the reduction of primary imines, which are intermediates to obtain primary amines. Due to the instability and high reactivity of primary imine, its reduction is difficult compared to secondary imine. Thus, the catalyst works for the synthesis of primary amines, generally applicable for secondary and tertiary amines too. Interestingly, our Fe-based single atom catalysts exhibited high selectivity towards the synthesis primary amines as well as secondary and tertiary amines (Scheme S1).

Results and Discussion

Preparation of Fe-Based Materials and Evaluation of their Catalytic Performances

To ensure sufficiently reactive and creation of stable catalytic centers, highly dispersed iron species were generated on nitrogen-doped carbon (Figure 1). For this purpose, colloidal silica (LUDOX®HS-40; 40 wt % suspension in H_2O) was mixed in ethanol at 60 °C with different amine ligands (aniline **L1**; p-phenylenediamine **L2**, PPD; o-phenylenediamine **L3**, OPD; m-phenylenediamine **L4**, MPD; and hexamethylenediamine **L5**, HMD). After 1 h, $FeCl_3 \cdot 6H_2O$ was added and stirred for 20 h. Then, the solvent was removed, and the resulting solid was dried and pyrolyzed under argon at different temperatures (400–1000 °C) for 2 h. Finally, the silica template and residual larger iron nanoparticles were removed by etching with ammonium hydrogen fluoride (5 M NH_4HF_2) and washing with 1 M HNO_3 solution (Figure 1). The resulting materials are represented as Fe-L@NC-T; where L and T represent ligand and pyrolysis temperature, respectively. It should be noted that all precursors used for this preparation are inexpensive and available on a large scale.

Next, all Fe-based materials (Fe-L@NC-T) were tested for the reductive amination of furfural **1** with gaseous ammonia to obtain furfurylamine **2** in the presence of molecular hydrogen as a benchmark reaction. Furfural is a renewable feedstock, and the desired bio-based product is

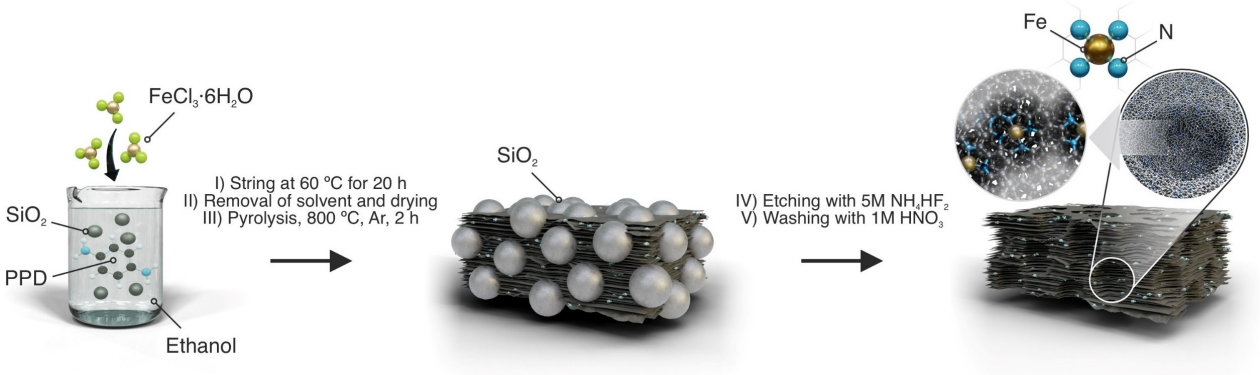

Figure 1. Schematic representation for the synthesis of single atom Fe-catalyst with mesoporous N-doped carbon support.

used for several industrial applications,[51–53] e.g. the synthesis of the pharmaceutical drug furtrethonium. As shown in Table 1, among the tested catalysts the one prepared from **L2** displayed the best performance (99 % conversion; 85 % yield of furfurylamine **2**; Table 1, entry 2). Apart from the desired product, a small amount of the secondary imine was formed. Other materials obtained from **L1**, **L3**, **L4** or **L5** showed lower activities and selectivities (Table 1, entries 1, 3–5). To evaluate the optimal pyrolysis temperature, materials Fe-L2@NC-T prepared at 400, 600, 800 and 1000 °C were tested in the model reaction (Table 1, entries 2, 6–8). On increasing the pyrolysis temperature from 400–800 °C both activity and selectivity of these materials also increased. However, at higher temperature (1000 °C) the respective material showed less activity and selectivity. Other materials containing SiO_2 and the one prepared without ligand as well as the homogeneous complexes exhibited significantly lower performance. Detailed optimization of critical reaction parameters is shown in Tables S4–5.

Characterization of Fe-Based Single Atom Catalysts

To understand the structural features of the prepared single atom catalysts and to establish a structure–activity relationship, the optimum catalyst (Fe-L2@NC-800), the catalyst before silica removal (Fe-L2@NC-SiO_2-800) as well as a recycled catalyst (Fe-L2@NC-800-R, after one run) were characterized using X-ray powder diffraction (XRD), high resolution transmission electron microscopy (HRTEM), high-angle annular dark-field scanning TEM (HAADF-STEM), energy dispersive X-ray spectroscopy (EDS), X-ray photoelectron spectroscopy (XPS), Mössbauer spectroscopy, inductively coupled plasma optical emission spectroscopy (ICP-OES), extended X-ray absorption fine structure (EXAFS) and X-ray absorption near edge structure spectroscopy (XANES) data collection.

Table 1: Fe-catalyzed reductive amination furfural with ammonia in presence of molecular hydrogen.

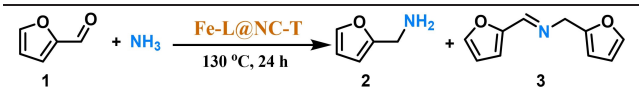

1 2 3

Entry	Catalyst	Conv. 1 (%)	Yield. 2 (%)	Yield. 3 (%)
1	Fe-L1@NC-800	70	50	14
2	Fe-L2@NC-800	>99	85	10
3	Fe-L3@NC-800	81	68	12
4	Fe-L4@NC-800	89	77	10
5	Fe-L5@NC-800	61	35	20
6	Fe-L2@NC-400	40	28	10
7	Fe-L2@NC-600	77	62	12
8	Fe-L2@NC-1000	88	71	15
9	Fe-L2@SiO_2-800 (Remaining SiO_2)	15	6	7
10	Fe@SiO_2-800 (Without ligand)	36	21	13
11	$FeCl_3{\cdot}6H_2O$ + L2	10	2	7
12	$FeCl_3{\cdot}6H_2O$	8	2	5

Reaction conditions: 0.5 mmol furfural, 50 mg Fe-catalyst (1.5–2.0 mol% Fe), 5 bar NH_3, 40 bar H_2, 2 mL MeOH, 130 °C, 24 h. For homogeneous catalysis conditions: 10 mol% of $FeCl_3{\cdot}6H_2O$ and 30 mol% of ligand were used. Conversions and yields were determined by GC using n-hexadecane standard.

The XRD patterns of these three materials are quite similar and indicate the dominant presence of two distinct diffraction peaks around 26° and 44°, which show similarities to the (002) and (100) crystal planes of graphitic carbon and graphene/graphite oxide, respectively (Figure S2)[54] but show a rather large broadening possibly due to a lack of long-range order. There are no diffraction peaks related to crystalline metallic iron or iron oxides in any of these materials, indicating that iron species are well dispersed in the carbon matrix, and they are not present in the form of nanoparticles as expected also due to very low content of iron. Indeed, the contents of Fe in the optimal catalyst (Fe-L2@NC-800) and recycled catalyst (Fe-L2@NC-800-R) were determined by ICP-OES to be approximately 0.95 wt % and 0.93 wt %, respectively.

HAADF-STEM images of all three catalysts are shown in Figure 2. Importantly, both fresh optimal catalyst Fe-L2@NC-800 (Figure 2e) and the recycled one Fe-L2@NC-800-R (Figure 2f) exhibited similar highly porous carbon structure with the presence of single Fe atoms. In the recycled material, very low amounts of Fe atomic clusters were also observed indicating a partial agglomeration of single atom centers with reaction time.

The porosity of fresh and recycled catalysts (Figure 2b and c) clearly stems from the removal of SiO_2 as proved by the comparison of adsorption and desorption isotherms of both samples (Figure S1). Indeed, adsorption desorption isotherms confirm the highly mesoporous nature of the sample exhibiting a large surface area of 509 m^2/g (Table. S1). The pore size distribution corresponds well with the size distribution of original silica nanoparticles showing the maximum at 6 nm. Meanwhile, EDS analyses of the fresh and recycled catalyst also confirm the presence of Fe in all the samples (Figs. S4 and S6). The high-resolution HAADF-STEM images of fresh and recycled catalysts show the single Fe atoms (Figure 2e and f, marked arrows and Figure S5a) which cannot be seen in Fe-L2@NC-800-SiO_2 due to SiO_2 dominating the contrast (Figure 2d). Annular bright field (ABF) STEM images corresponding to the HAADF images in Figure 2 showing the carbon pore structure can be found in Figure S7. The nature and size of pores in optimum catalyst are clearly seen in representative HRTEM image in Figure S5b.

Next, XPS was used to determine the surface elemental compositions and electronic state of Fe-L2@NC-800 and Fe-L2@NC-800-R catalysts. The survey spectra of both fresh and recycled catalysts exhibited distinctive peaks of C, N, O, Fe and Si, the latter one in small amounts remaining from the preparation process of the catalyst (Table S2 and Figure S8). The elemental quantification in Table S2 reveals a Fe surface concentration of 0.2 at. % for both catalysts whereas N can be found with 9.2 and 7.8 at. % for Fe-L2@NC-800 and Fe-L2@NC-800-R, respectively. High-resolution N 1s spectra (Figure 3a and Figure S9) of both samples displayed five peaks at binding energies of 398.3,

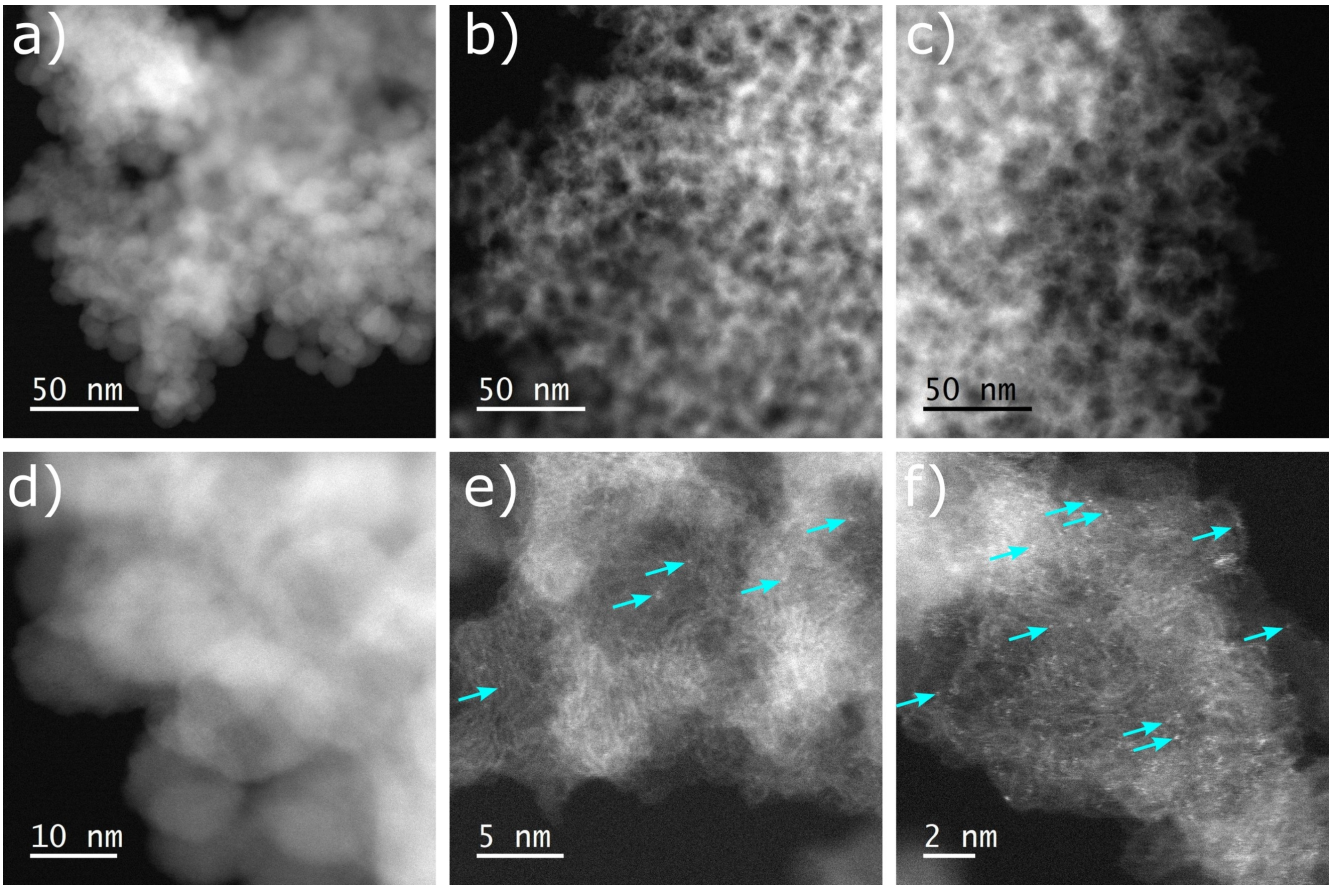

Figure 2. Overview (upper row) and high resolution (lower row) HAADF-STEM images of Fe-L2@NC-800-SiO_2 (a, d), Fe-L2@NC-800 (b, e) and Fe-L2@NC-800-R (c, f) showing the general morphology with the similarity between the size of the SiO_2 particles and the size of pores in catalysts after SiO_2 removal.

399.9, 401.0, and 402.8 eV corresponding to pyridinic and/or Metal-Nx species, pyrrolic, graphitic, and oxidized pyridinic N species,[55–56] respectively, as well as a peak at 405.7 eV which corresponds to nitrate species probably from the SiO_2 removal process. However, besides a reduction of the nitrate peak the spectra of the fresh and recycled catalysts are rather comparable. High-resolution Fe 2p spectra of both samples are also very similar (Figure 3b and Figure S9) and suggests the presence of several Fe species. The peaks at 708.5 and 721.8 eV suggest the presence of Fe^{2+} whereas the peaks at 710.7 and 723.8 eV as well as at 713.2 and 726.6 eV can be connected to Fe^{3+} and Fe-Nx species.[57–58] The pronounced satellite peaks at 716.3 and 729.6 eV are probably caused by the overlap of typical Fe^{2+} and Fe^{3+} satellite features.[57] XPS suggests that iron species might be present in both fresh and recycled catalysts in the form of single iron(II) and iron(III) atoms embedded in the Fe–N–C local environment. Nearly the same character of high-resolution N 1s and Fe 2p spectra of Fe-L2@NC-800 and Fe-L2@NC-800-R catalysts manifests that the local environment of iron is well preserved after recycling. To investigate the local surroundings, coordination, and electronic properties of iron species, Mössbauer spectroscopy and X-ray absorption spectroscopy (XAS) were used for further characterization.

The room temperature ^{57}Fe Mössbauer spectrum of Fe-L2@NC-800 shows two doublet components (Figure 3c). Based on the derived hyperfine parameters, the doublet with the lower values of the isomer shifts and quadrupole splitting parameters (0.39 and 1.05 mm/s, respectively) is attributed to Fe^{3+} ions in a high-spin state ($S=5/2$). The other doublet with increased isomer shift value (0.46 mm/s) and significantly higher quadrupole splitting (2.55 mm/s) can be assigned to Fe^{2+} ions in the spin-state of $S=2$. The large value of quadrupole splitting reflects the high asymmetry of local surroundings of probed Fe^{2+} atoms as typical for tetrahedral iron(II) coordination in e.g. Fe^{2+} phthalocyanines with Fe-N_4 local environment. Indeed, the hyperfine parameters of the Fe^{2+} doublet in Mössbauer spectrum of Fe-L2@NC-800 sample are in the perfect correlation with those measured for iron(II)-phthalocyanine.[59–60]

To further elucidate the valence state and local coordination structure of iron sites in the optimum Fe-L2@NC-800 catalyst, X-ray absorption spectroscopy experiments at the Fe K-edge were performed. The X-ray absorption near edge structure (XANES) spectrum of Fe-L2@NC-800 (Figure 3d) reveals a K-edge energy of 7122.9 eV, which indicates

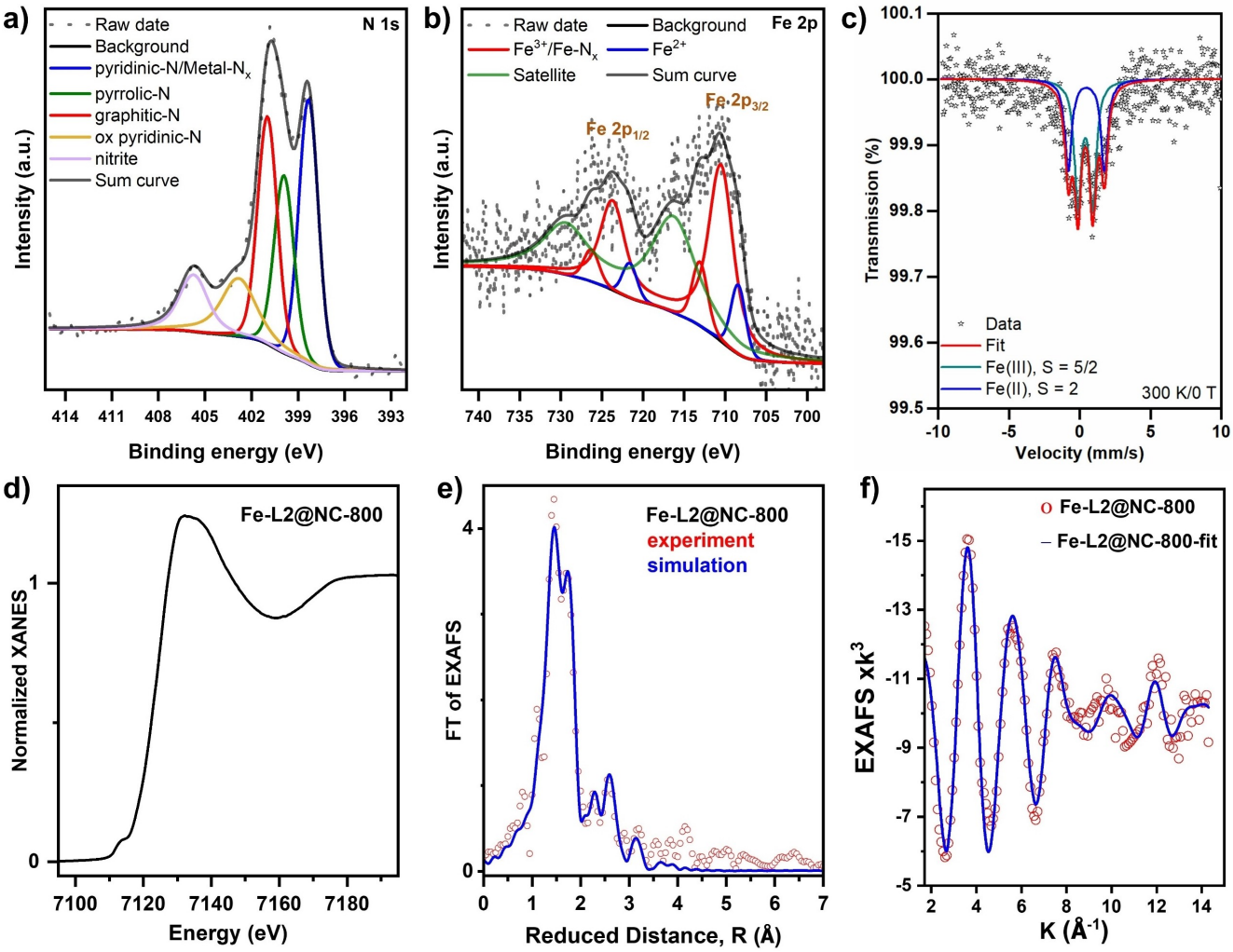

Figure 3. XPS and XAS data for Fe-L2@NC-800. High resolution XPS in the (a) N 1s region and (b) Fe 2p region. (c) ^{57}Fe Mössbauer spectrum. (d) XANES spectrum at the Fe K-edge (K-edge energy at 50% level 7122.0±0.1 eV), (e) Fourier-transform of EXAFS spectrum in (f) (solid lines, simulation; circles, experimental data).

presumably similar amounts of Fe^{2+} and Fe^{3+} species, i.e., in comparison to XANES spectra of $Fe^{II}O$ and $Fe^{III}_2O_3$ (Figure S10). The relatively small pre-edge feature (~7112.5 eV) suggests relatively centro-symmetric iron sites and the shallow K-edge slope, and small white-line amplitude point to a low coordination number. The Fourier-transformed extended X-ray absorption fine structure (EXAFS) spectrum (Figure 3e) shows two resolved short-distance peak features, due to 1st-sphere ligands at iron and smaller peak features at larger distances below 3 Å. EXAFS simulation analysis revealed two discernable iron-ligand bond lengths of ca. 1.90 Å and 2.10 Å with a coordination number each of close to 2, suggesting mostly 4-coordinated iron sites, as well as small numbers of longer Fe–C distances (ca. 3–3.5 Å) (Table S3). The longer or shorter Fe–N or Fe–O bonds are likely attributable mostly to either Fe^{2+} or Fe^{3+} sites. We note that nitrogen or oxygen bonding of iron cannot be distinguished in EXAFS simulations due to similar Z-values of these elements. Importantly, Fe–Fe distances were barely discernable, confirming the dominant presence of isolated single-atom iron sites in Fe-L2@NC-800. The EXAFS results are well compatible with tetrahedral iron sites with 4 nitrogen ligands surrounded by several C-atoms in the Fe-L2@NC-800 catalyst, but do not exclude other types of coordination including oxygen bonds. Treatment of Fe-L2@NC-800 with O_2 resulted in a ca. 1.3 eV K-edge up-shift, suggesting almost complete oxidation to Fe^{3+}. This notion was supported by the overall shortening by of the Fe–N bonds determined by EXAFS, which, however, also revealed an increase in the 1st-sphere ligands coordination number, suggesting limited oxygen species binding at iron (Figure S10 and Table S3). Treatment of a pre-oxidized Fe-L2@NC-800 sample with H_2 resulted in a ca. 0.5 eV K-edge down-shift vs. the untreated material, due to minor iron reduction, while the Fe–N bonds remained similar to the O_2-treated sample (Figure S10 and Table S3).

In summary, we propose that the optimal catalyst, Fe-L2@NC-800 contains ca 1 wt% of iron species, which are mainly in the form of isolated Fe^{2+} and Fe^{3+} atoms, which are responsible for unique catalytic activity and selectivity of

Fe-L2@NC-800 in reductive aminations. To confirm the active species, the optimal catalyst, Fe-L2@NC-800 was subjected to reduction with molecular hydrogen and oxidation with air. The reduced material with H_2 (Fe-L2@NC-800-H_2), which contains mainly Fe^{2+} species, exhibited slightly higher activity and selectivity than that of the optimal catalyst (89 % yield of **2**). However, the one calcined in air, which contains larger amounts of Fe^{3+} species, resulted in a less active and selective material. These experiments indicate that the most active catalytic species are iron(II) single ions tetrahedrally coordinated with nitrogen atoms in N-doped porous graphitic support. Importantly, the highly mesoporous structure and local coordination of iron species are preserved after the catalyst recycling (Figure 2c and Figure S9). The combination of single iron atoms sitting in Fe-N_xO_x environments, and the highly mesoporous character of a carbon matrix seem to be crucial factors contributing to the high activity and selectivity of the developed catalyst. With respect to the reaction pathway of reductive amination reaction, first the carbonyl compound condenses with ammonia or amine and produces corresponding primary imine or secondary imine as intermediates.[46] These imine-based intermediates proceed to hydrogenation in the presence of Fe-L2@NC-800 to produce the desired product- primary or secondary amine. It should be noted that primary imine is unstable, and it is impossible to detect it; however, the corresponding secondary imine is quite stable, and it was identified during the reaction.[46]

Selective Synthesis of Primary, Secondary, and Tertiary Amines with Fe-L2@NC-800

For introducing new catalysts, specifically heterogeneous ones, their applicability to a broad range of substrates including multi-functionalized and sensitive ones, must be demonstrated. Initially, various primary amines were prepared starting from carbonyl compounds and simple ammonia (Scheme 1). The resulting products can be easily further functionalized and therefore represent central building blocks in organic chemistry. In this transformation, a general problem is chemoselectivity avoiding the formation of secondary and tertiary amines. To our delight, applying Fe-L2@NC-800 the reductive amination of aldehydes to benzylic, heterocyclic, and aliphatic linear primary amines proceeded in good to excellent yields (up to 90 %) with high selectivities (Scheme 1A). Sensitive functional groups including halides, cyano, esters, and amide as well as S-, N- and O-heterocycles are well tolerated (Scheme 1; products **5**–**12**, **16**–**24**). Compared to benzaldehydes, the reductive amination of aliphatic aldehydes is hampered by undesired aldol condensation, which easily occurs under basic conditions. Nevertheless, several aliphatic and araliphatic substrates gave the corresponding primary amines in good yields (up to 80 %) and high selectivity (Scheme 1; products **23**–**26**). The hydrogenation of the in situ generated imine from aldehydes is faster than that of the corresponding ketone-derived imines. Thus, a more active catalyst or more drastic conditions are required for efficient reductive amination of ketones. Interestingly, both industrially relevant and structurally challenging ketones underwent smooth amination in the presence of Fe-L2@NC-800 and produced the corresponding branched primary amines in good to excellent yields (Scheme 1B).

Next, we explored the synthesis of secondary and tertiary amines (Scheme 2). As expected, different amines reacted with aldehydes to give the corresponding secondary amines selectively in up to 85 % yield (Scheme 2A; products **40**–**60**). As an example, the reductive alkylation of N-containing heterocycles as well as primary and secondary amines gave the corresponding derivatives in 67–85 % yields (Scheme 2A; products **50**–**53**). Like aldehydes, diverse ketones were reacted with various amines and produced the corresponding secondary amines in 61–88 % (Scheme 2B; products **61**–**78**). In general, for most reductive amination reactions high chemoselectivity is observed. However, in a few cases, e.g. **59**, **65** and **75**, we observed minor amounts of the corresponding alcohol (< 5 %) and/or secondary imine/amine (< 10 %).

Among the various alkylated amines, N-methylamines are of special interest because of their role in regulating biological functions.[61–62] In general, this class of amines is prepared either through catalytic reductive amination with formaldehyde[46,63] or by using (toxic) methylation reagents.[61–62] By applying our single atom Fe catalyst, we prepared selected *N*-methylamines starting from aldehydes and *N*,*N*-dimethylamine (DMA), which is a readily available bulk chemical (Scheme 3A; products **79**–**94**). In addition, the direct reductive methylation of amines with aqueous formaldehyde produced selectively the corresponding *N*-methylamines (Scheme 3B; products **95**–**106**).

Synthetic Applications to Chiral Products, Biomolecules, and Late-Stage Drug Functionalization

To showcase the potential of the presented Fe catalyst in modern organic chemistry, we investigated its performance in important synthetic applications. In this respect, the functionalization of chiral molecules was studied at first. As shown in Scheme 4A, N-alkylation of chiral primary and secondary amines with different aldehydes took place smoothly in the presence of molecular hydrogen to achieve N-alkylated chiral secondary and tertiary amines with good yields. Notably, under the reaction conditions the enantiomeric excess (ee) of substrates and products is comparable. For example, primary amines such as (R)-1-(4-chlorophenyl)ethan-1-amine and (R)-1-(naphthalen-2-yl)ethan-1-amine reacted selectively with substituted aryl aldehydes to form the chiral benzyl amines in up to 80 % yield and 99 % ee (Scheme 4A; products **107**–**108**). In addition, araliphatic and aliphatic amine led to reductive coupling with benzaldehydes and provided the corresponding chiral amines in up to 73 yield and 99 % ee (Scheme 4A; products **110**–**113**).

Furthermore, (R)-1-(naphthalen-1-yl)ethan-1-amine provided the drug cinacalcet in 71 % yield and 99 % ee

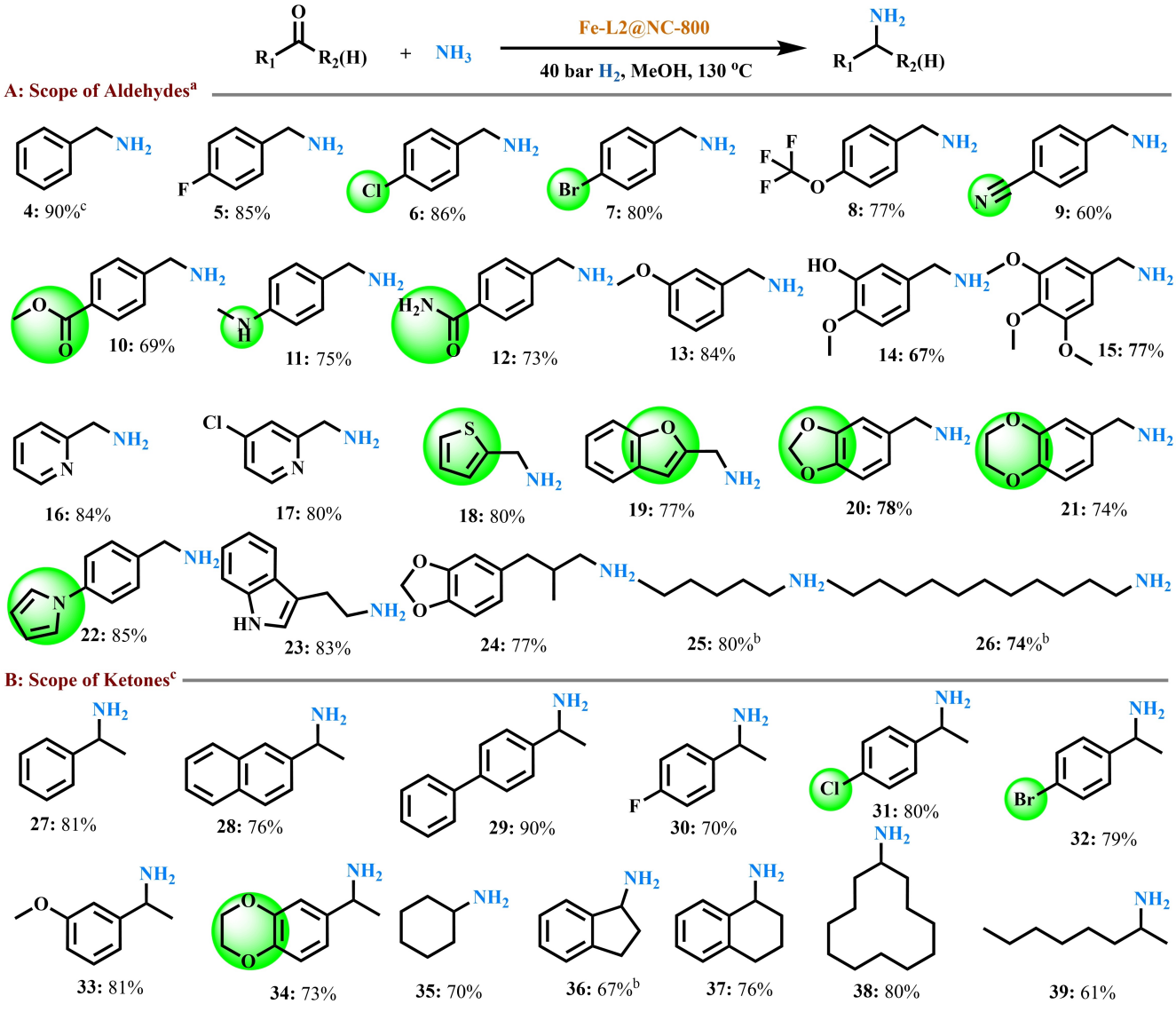

Scheme 1. Fe-L2@NC-800 catalyzed synthesis of primary amines from aldehydes and ketones with ammonia.[a] [a] Reaction conditions: 0.5 mmol aldehydes, 50 mg Fe-L2@NC-800 (1.70 mol% Fe), 40 bar H_2, 5 bar NH_3, 2 mL MeOH, 130 °C, 24 h, isolated yields. [b]GC yield. [c] same as "a" with 0.5 mmol ketones at 140 °C. The primary amines were isolated by chromatography and converted to their corresponding hydrochloride salts for measuring NMR and HRMS.

(Scheme 4A; product **109**). The reductive amination of amino acid derivates offers a straightforward methodology for the modification of peptides and proteins. Nevertheless, such reactions have been less explored compared to other reductive aminations.[45–47] As an example, the reaction of methyl L-phenylalaninate with 4-fluorobenzaldehyde provided the N-alkylated amino acid ester in 88% yield and 89% ee (Scheme 4A; product **114**). The amination of ketones with chiral amines leads to diastereomeric secondary amines in moderate to good yields (Scheme 4B; products **115**–**119**). In the case of α-chiral amines and aromatic ketones good diastereomeric ratios (dr) from 86:14 to 59:41 were obtained, while lower induction was observed in the case of β-chiral amines and aliphatic ketones.

Next, the versatility of this methodology is showcased in the preparation of 13 existing drug molecules (Scheme 5; products **120**–**132**) for different kinds of medical treatments. The desired molecules were synthesized in part in multi g-scale and yielded up to 87%. In addition, this catalyst system allows the introduction of -NH_2 moieties into complex molecules and drugs. Exemplarily, the amination of raspberry ketone, zingerone, and azaperone (Scheme 5; products **133**–**134**, **136**) as well as steroid derivatives were demonstrated (Scheme 5; products **135**, **137**). Remarkably, in the presence of a nearby chiral center high diastereoselectivity can be achieved (Scheme 5; product **135**). Notably, N-alkylated amino acid derivatives are widely distributed in nature, and such molecules are found in modern pharmaceuticals such as Cilazapril and Enalapril, as they trigger

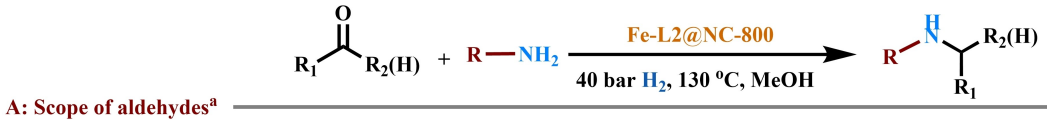

A: Scope of aldehydes[a]

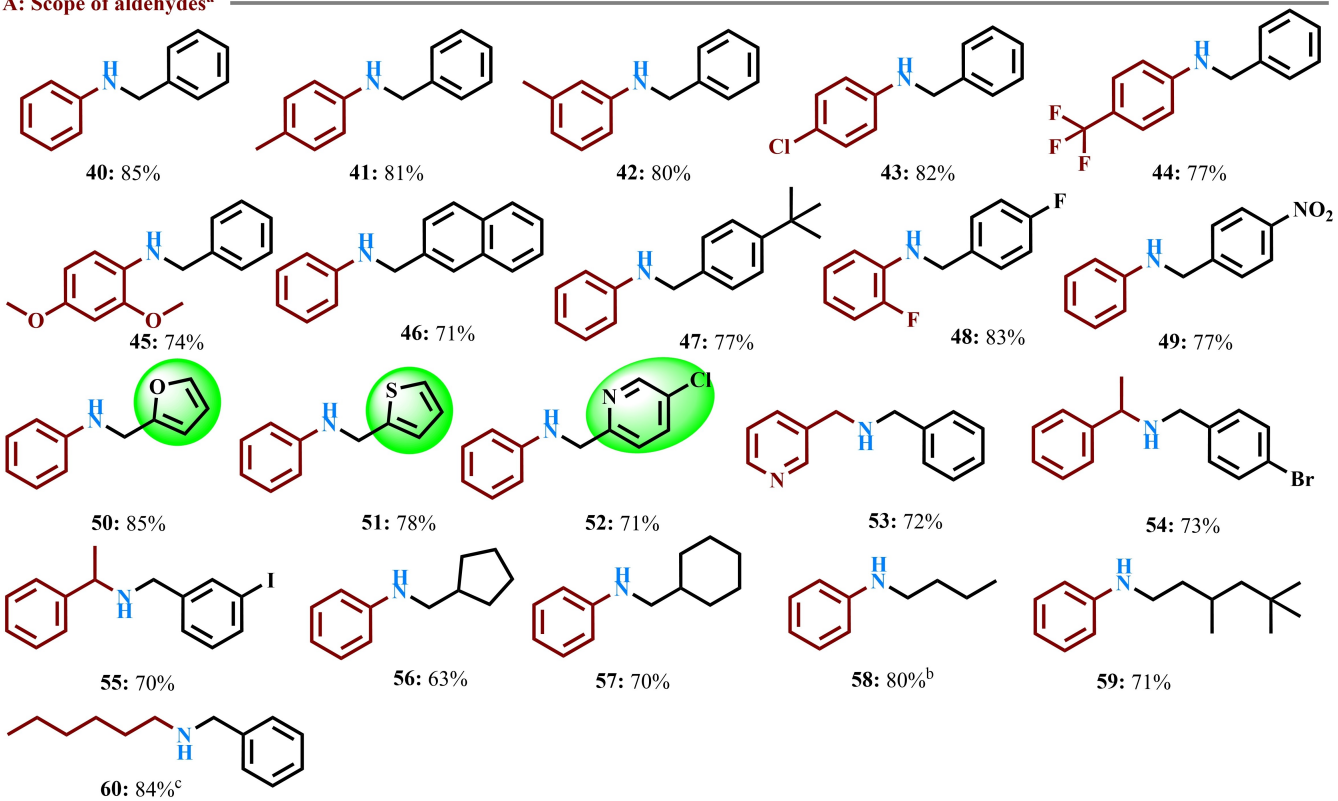

B: Scope of ketones[c]

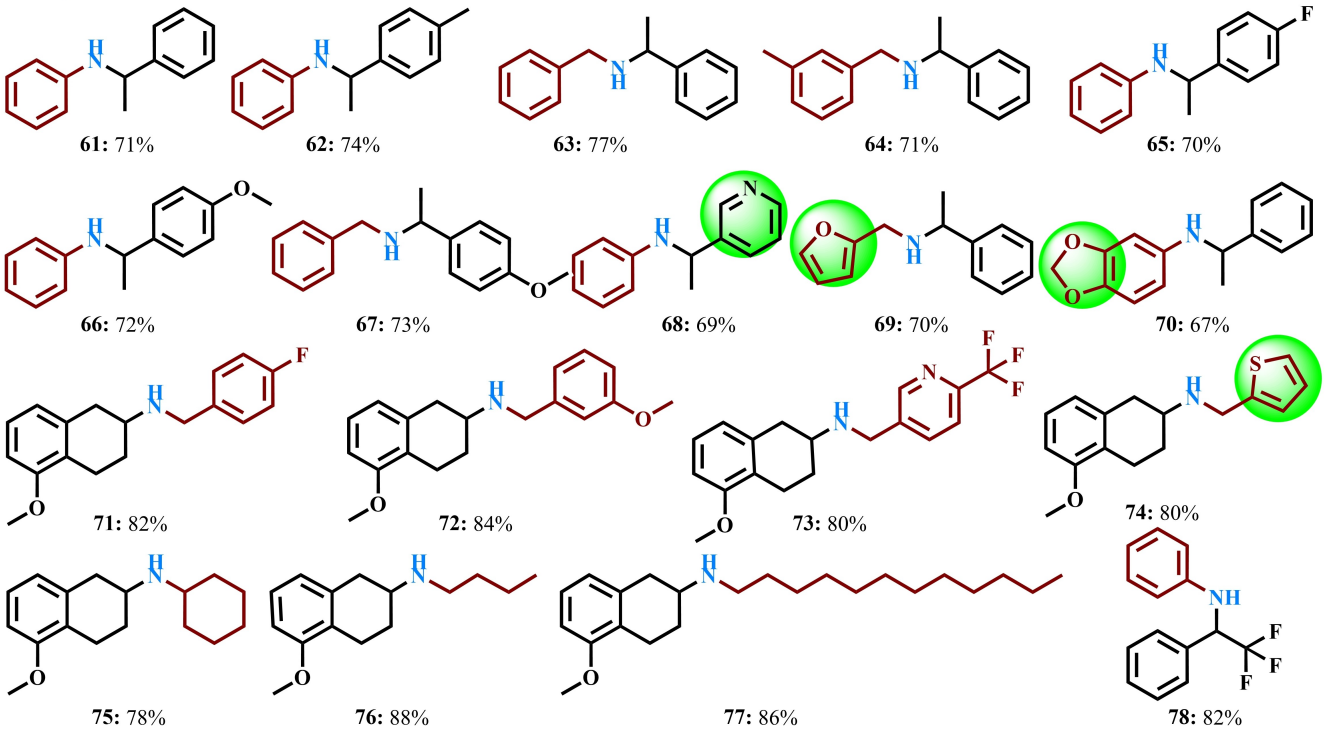

Scheme 2. Synthesis of secondary and tertiary amines using Fe-L2@NC-800. Reaction conditions: 0.5 mmol amines, 0.7 mmol aldehydes, 50 mg Fe-L2@NC-800 (1.70 mol% Fe), 40 bar H_2, 2 mL MeOH, 130 °C, 24 h, isolated yields. [c] same as "a" with 0.5 mmol amines, 0.7 mmol ketones, 140 °C. [b] GC yield.

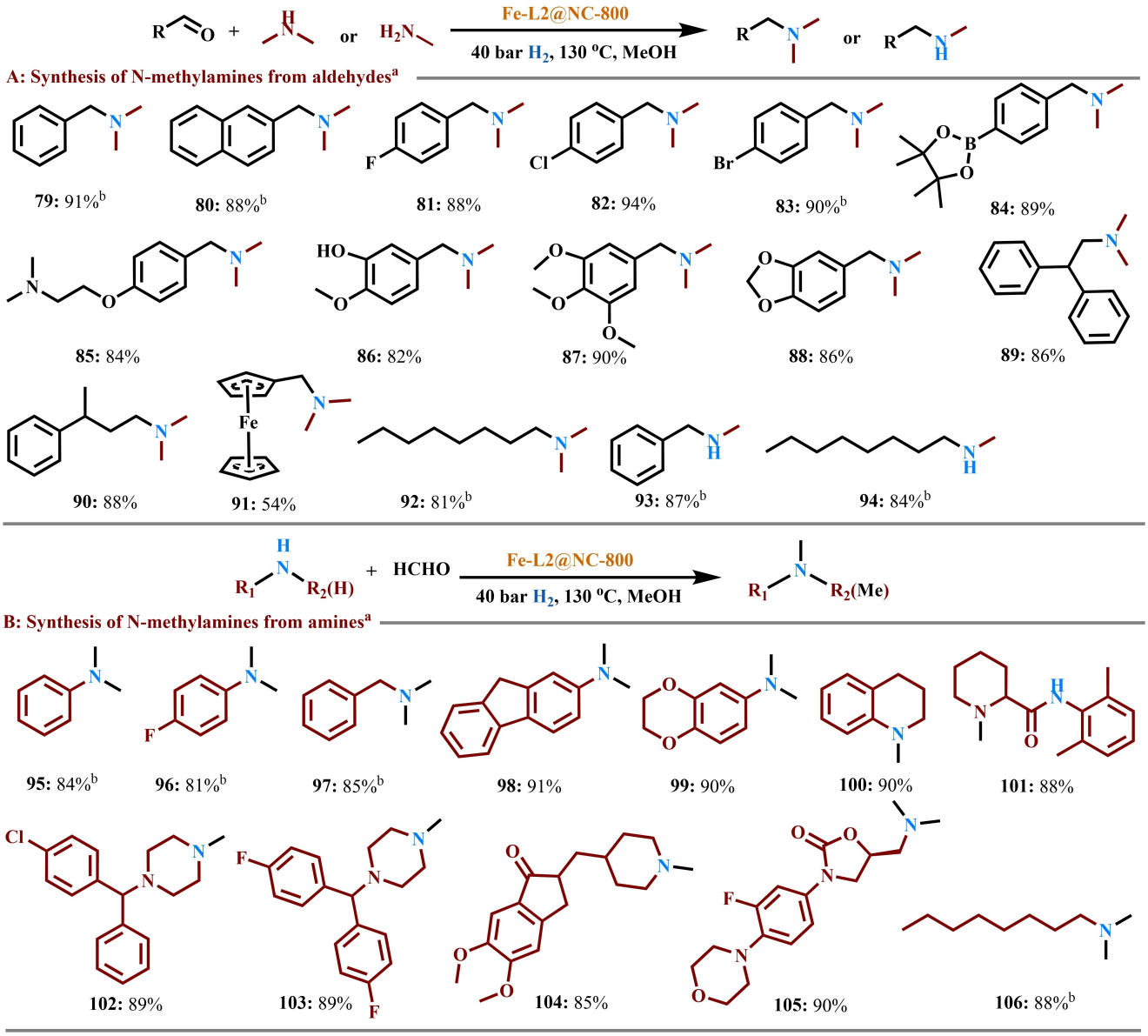

Scheme 3. Synthesis of N-methylated amines from aldehydes and ketones applying Fe-L2@NC-800. ***A:*** Reactions of aldehydes with dimethylamine. [a] Conditions are 0.5 mmol aldehyde, 1 mL aqueous dimethylamine (1 M), 40 mg Fe-L2@NC-800 (1.36 mol% Fe), 1 mL MeOH, 120 °C, 24 h, isolated yields; [b] GC yield. ***B:*** Reactions of amines with formaldehyde. [a] Conditions are 0.5 mmol amines, 100 µL aqueous formaldehyde (37%), 40 mg Fe-L2@NC-800 (1.36 mol% Fe), 2 mL MeOH, 120 °C, 24 h, isolated yields; [b] GC yield.

many biological processes. Compared with standard amines, the reductive alkylation of this class of compounds is more demanding. Nevertheless, benzylic, heterocyclic as well as multi-substituted amines reacted smoothly with methyl or ethyl phenylglyoxylate and gave the corresponding α-amino acid esters in up to 92 % yield (Scheme 6; products **141**–**158**). The shown halogenated and functionalized α-amino acid esters offer possibilities for further valuable transformations. Similarly, different functional groups such as hydroxyl-, ether-, thioether-, ester-, amide-, fluorenyl-containing anilines as well as heterocyclic amines provided the respective functionalized amino acid esters, e.g. **149**, **154**–**173**.

Next, we explored the scope of α-keto esters, and a series of substituted and functionalized amine acid esters were prepared. The reductive amination of methyl pyruvate and ethyl 2-oxovalerate with various anilines including secondary amines led to desired products in high yield (Scheme 6; products **174**–**177**, **205**–**207**). Similarly, different substituted aryl keto esters including halogenated ones (F–, Cl–, Br–, CF_3–) as well as (thio)ether-, thiophene-, and di-substituted substrates provided the corresponding products in up to 92 % yield (Scheme 6; products **178**–**182**, **199**–**204**).

After successfully preparing a series of amino acid esters, we turned to our research interest in the synthesis of different amino acid amides. Firstly, we tried to use 1.0

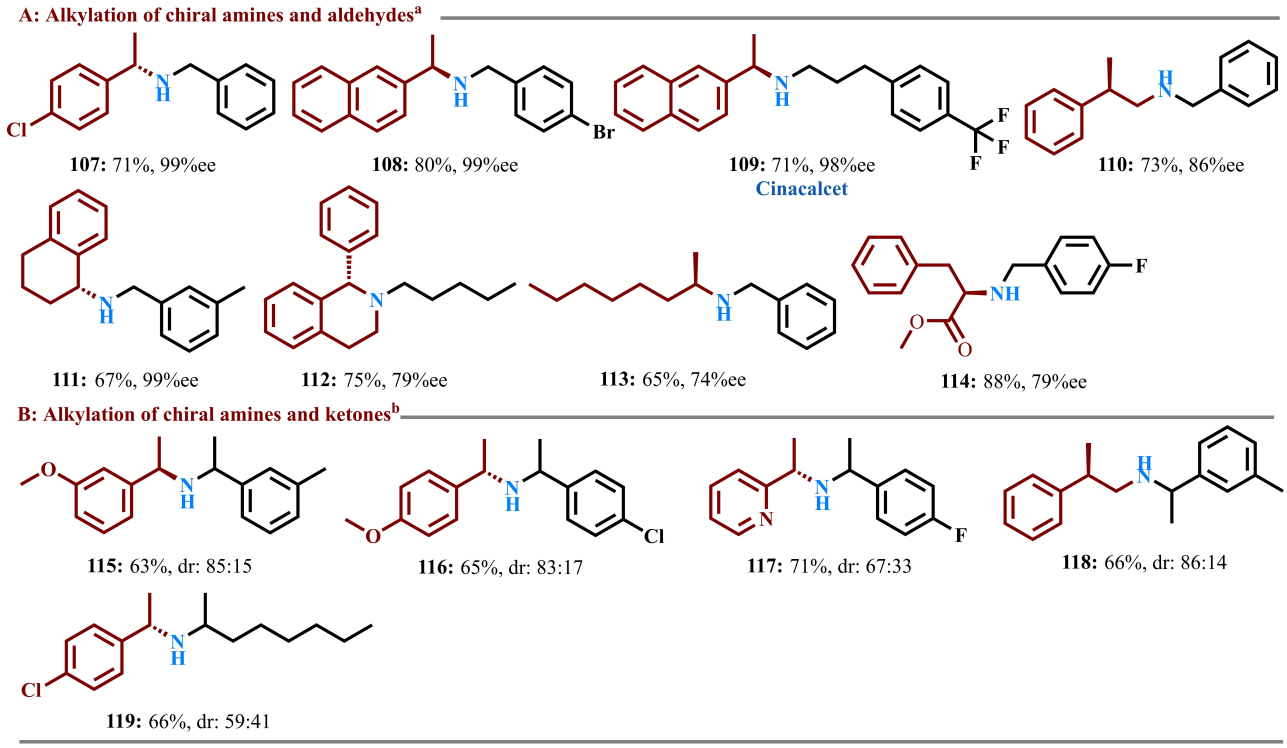

Scheme 4. Fe-L2@NC-800 catalyzed synthesis of chiral products.[a] [a] Reaction conditions: 0.5 mmol amine, 0.7 mmol carbonyl compounds, 50 mg Fe-L2@NC-800 (1.70 mol% Fe), 40 bar H_2, 2 mL MeOH, 130 °C, 24 h, isolated yields. [b] same as "a" at 140 °C.

equiv. ethyl phenylacetate and 2.0 equiv. of aniline to synthesize corresponding amides under standard conditions. Unfortunately, our catalytic system did not give any desired product. However, it is worth noting that when we use n-octylamine instead of aniline, 93 % of the desired product can be achieved in the presence of 40 bar H_2 at 80 °C for 20 h in t-BuOH solvent (Scheme 7; product **208**). Furthermore, various substituted keto esters were also tested for the synthesis of amine acid amide by using n-octylamine as amine source and provided the corresponding products in up to 90 % yield (Scheme 7; products **209**–**217**). In addition, we also tried different amines as nucleophile reagents to synthesize asymmetric amine acid amides (Scheme 7; products **218**–**220**). Apart from the keto ester, we also tried to prepare α-amino acid amides from α-keto amides and anilines (Scheme 7; product **221**–**235**). To our delight, our catalytic system also exhibited high activity and selectivity for the reductive amination of α-keto amide.

Stability and Reusability of Fe-L2@NC-800 Catalyst

For any heterogeneous catalyst, its stability, recyclability, and reusability are key aspects to achieve chemical synthesis in a more cost-efficient manner. To check these features, we performed recycling experiments for the synthesis of ethyl 2-anilino-2-phenylacetate and furfurylamine at two different conversions (complete and around 50 %, respectively). As shown in Figure 4a, Fe-L2@NC-800 exhibited high stability and can be recycled and used seven times without a significant decrease in performance. However, using ammonia gas as a reagent, the catalyst displayed lower stability (Figure 4b). Hence, we assume that the type of amine has a significant effect on the long-term stability of the catalyst.

Conclusions

Here, we present the general strategy for the synthesis of single atom iron catalysts with highly mesoporous nitrogen-doped carbon support. The developed universal catalysts allow for the preparation of diverse primary, secondary, and tertiary amines including N-methylated products as well as life science molecules (pharmaceuticals, agrochemicals, amino acid derivatives) starting from carbonyl compounds and green hydrogen in good to excellent yields. Importantly, the recycled catalysts keep the mesoporous character, structural and electronic properties of active iron species, thus resulting in very good reusability. In this regard, the presented work demonstrates how non-noble single atom catalysis can contribute to the advancements in sustainable organic synthesis as well as the synthesis of life science molecules. Notably, in this amination process only water is produced as the byproduct. In addition, small amounts of imines or alcohols as side products are formed, which are also useful compounds. In this amines synthesis including selected pharmaceuticals, generation of any other waste or CO_2 was not occurred. Thus, this heterogeneous Fe-based reductive amination process is interesting not only for the

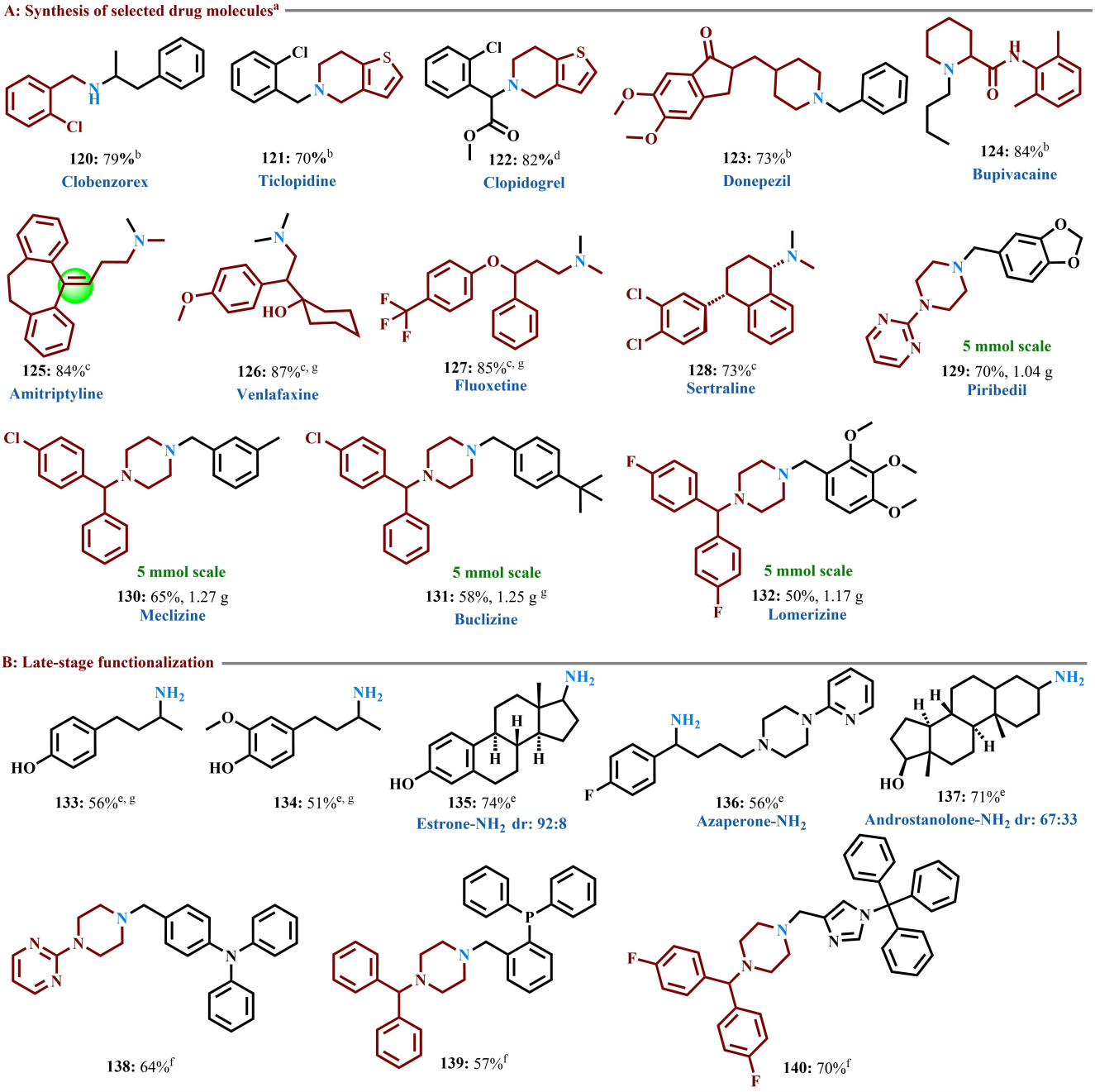

Scheme 5. Fe-L2@NC-800 catalyzed synthesis of selected drug molecules and late-stage functionalization of bio-active compounds.[a] [a] Reaction conditions: 5 mmol amines, 7 mmol aldehydes or ketones, 50 mg Fe-L2@NC-800 (1.70 mol% Fe), 40 bar H_2, 20 mL MeOH, 140 °C, 24 h, isolated yields. [b] Same as "a" with 0.5 mmol amine and 0.7 mmol aldehydes. [c] Reaction conditions: 0.5 mmol amines, 100 µL aqueous formaldehyde (37%), 40 mg Fe-L2@NC-800, 2 mL MeOH, 120 °C, 24 h. [d] Same as "b" with 100 °C with 40 mg Fe-L2@NC-800. [e] Reaction conditions: 0.5 mmol ketones, 5 bar NH_3, 50 mg Fe-L2@NC-800, 40 bar H_2, 2 mL MeOH, 140 °C, 24 h. [f] Same as "e" with 80 mg Fe-L2@NC-800 at 150 °C. ^{1}H NMR yield. [g] GC yield.

synthesis of essential products but also important for the advancement of waste- or CO_2-free industrial process.

Acknowledgements

We gratefully acknowledge the Deutsche Forschungsgemeinschaft (DFG; Project number 447724917), European Research Council and the State of Mecklenburg-Vorpommern for financial for general support. We also acknowledge the financial support from ERDF/ESF project TECHSCALE (No. CZ.02.01.01/00/22_008/0004587) and from the

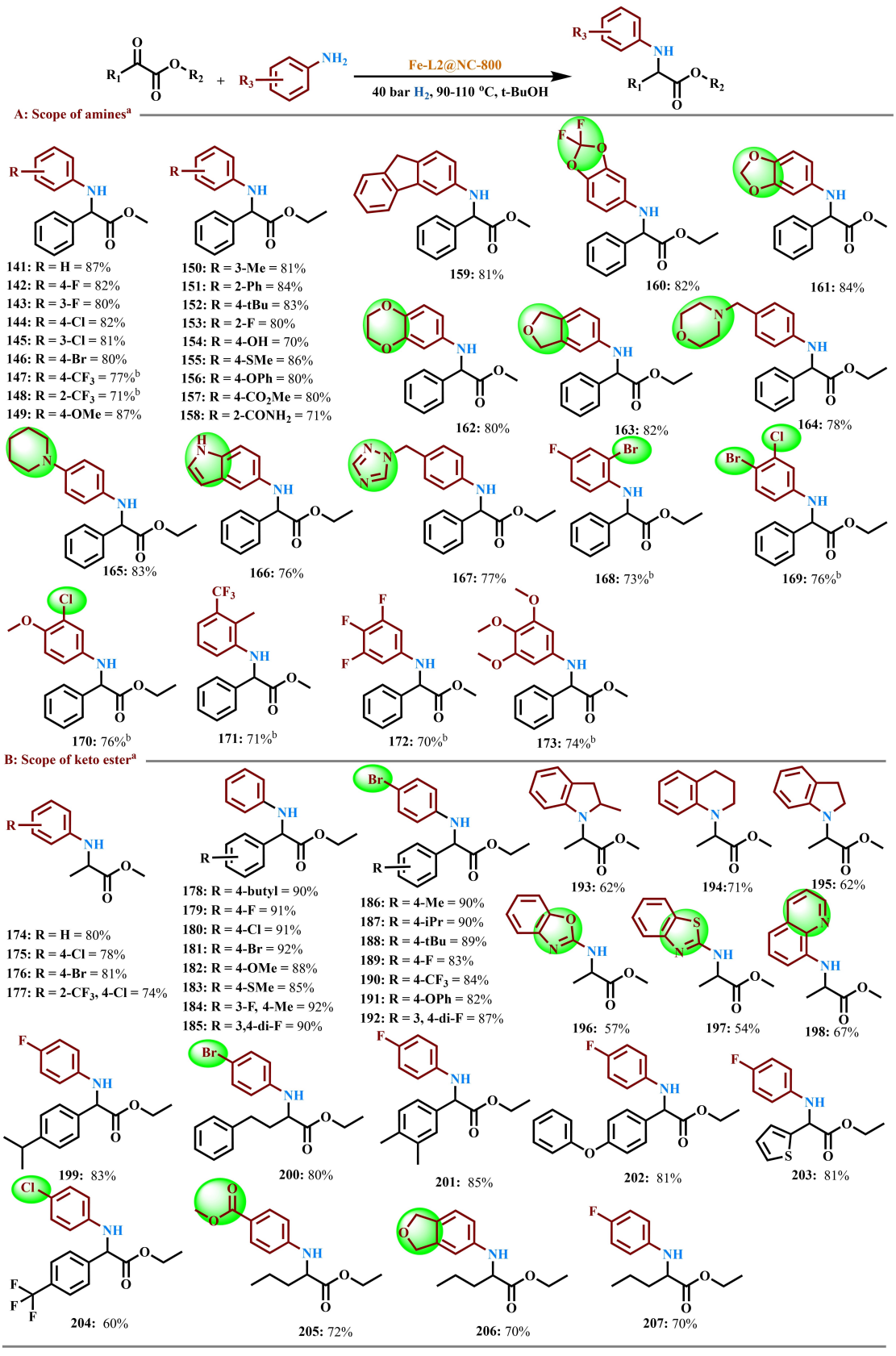

Scheme 6. Fe-L2@NC-800 catalyzed synthesis of α-amino acid esters from ethyl phenylacetate and different amines.[a] [a] Reaction conditions: 0.5 mmol ethyl phenylacetate, 0.7 mmol amine, 40 mg Fe-L2@NC-800 (1.36 mol% Fe), 2 mL t-BuOH, 90 °C, 20 h, isolated yields. [b] Same as 'a' with 110 °C.

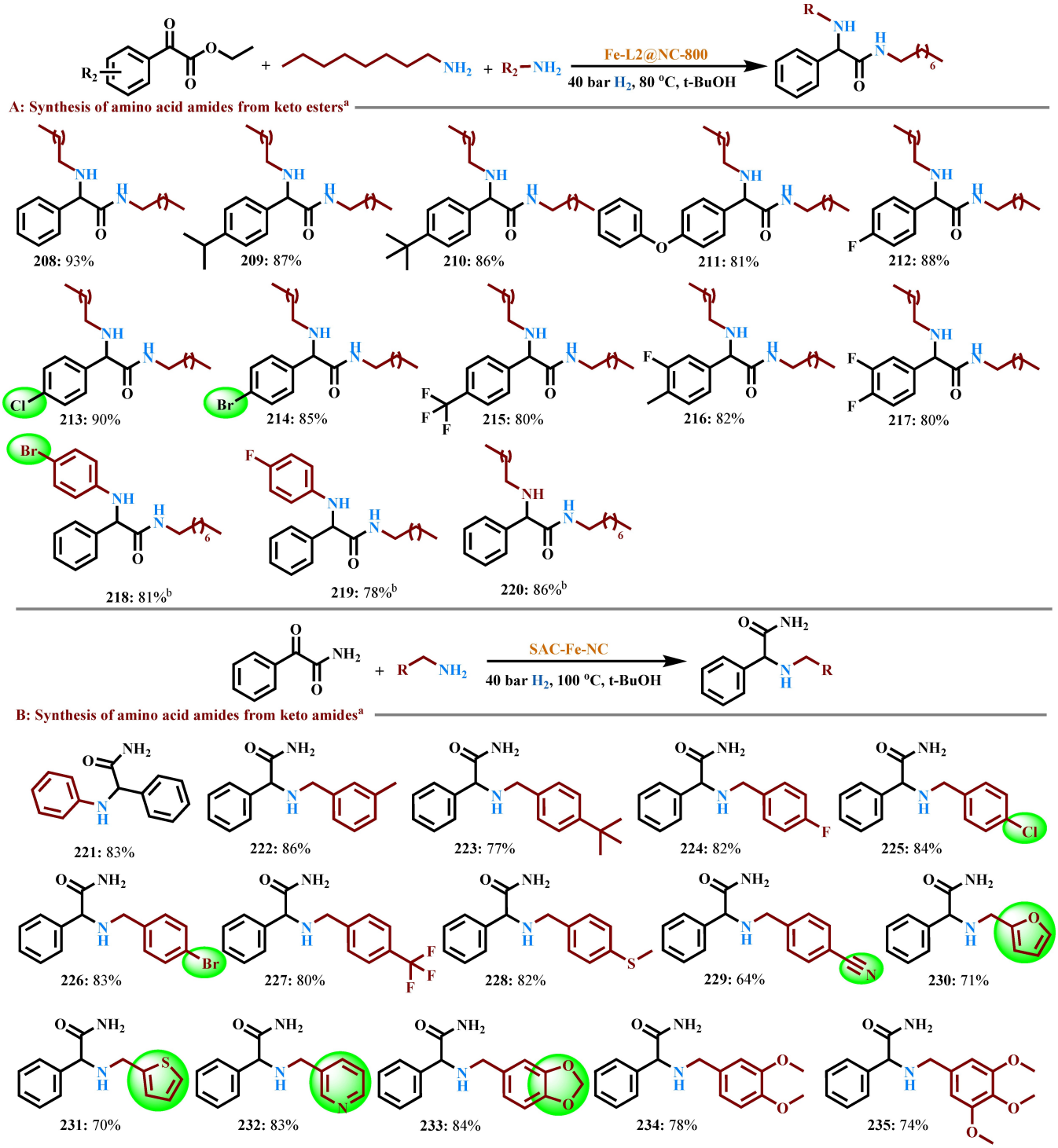

Scheme 7. Fe-L2@NC-800 catalyzed synthesis of α-amino acid amides from α-keto esters or α-keto amides and amines.[a] ***A:*** Reactions of amines with keto esters.[a] Conditions are 0.5 mmol keto ester, 0.7 mmol amine 1, 0.7 mmol amine 2, 40 mg Fe-L2@NC-800 (1.36 mol % Fe), 2 mL t-BuOH, 80 °C, 20 h, isolated yields.[b] same as "a" with 90 °C. ***B:*** Reactions of amines with keto amides. Conditions are 0.5 mmol keto amide, 0.5 mmol amines, 40 mg Fe-L2@NC-800 (1.36 mol% Fe), 2 mL t-BuOH, 100 °C, 24 h, isolated yields.

European Union under the REFRESH-Research Excellence For Region Sustainability and High-tech Industries project number CZ.10.03.01/00/22_003/0000048 via the Operational Programme Just Transition. Zhuang Ma thank the Chinese Scholarship Council (CSC) for financial support. The authors thank dr. Ondrej Tomanec and dr. Vojtěch Kupka from Palacky University in Olomouc for selected HRTEM and BET measurements and analytical team of the Leibniz-Institut für Katalyse e.V. for their excellent service. P. W. Menezes greatly acknowledges support from the

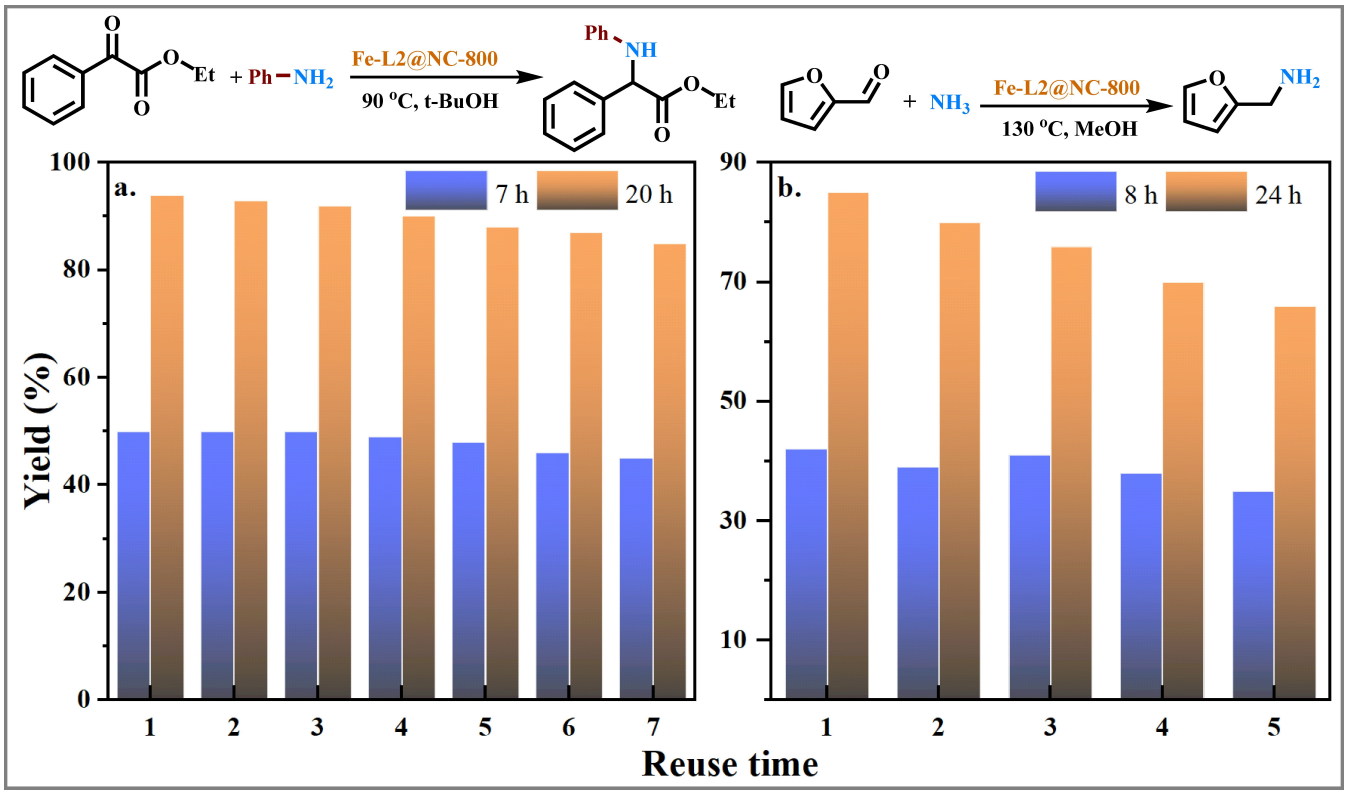

Figure 4. Stability and recycling of Fe-L2@NC-800 catalyst for the synthesis of ethyl 2-anilino-2-phenylacetate and furfurylamine, respectively. **a:** Reactions of amines with keto esters. [a] Conditions are 1 mmol ethyl phenylacetate, 1.4 mmol aniline, 80 mg Fe-L2@NC-800 (1.36 mol% Fe), 3 mL t-BuOH, 90 °C, 7 h and 20 h. **b**: Reactions of furfural amines with ammonia. Conditions are 1.0 mmol furfural, 5 bar NH_3, 100 mg Fe-L2@NC-800 (1.70 mol% Fe), 3 mL MeOH, 130 °C, 8 h and 24 h.

German Federal Ministry of Education and Research in the framework of the project Catlab (03EW0015 A/B). The authors thank the HZB for beamtime allocation at the KMC-3 synchrotron beamline of the BESSY synchrotron in Berlin-Adlershof.

MB and RVJ supervised the project. ZM, RVJ and MB planned and developed the project, and designed the experiments. ZM prepared catalysts and performed all catalytic experiments. CK (Chakreshwara Kuloor) involved in performing catalytic experiments. CK (Carsten Kreyenschulte) CK TEM measurement and analysis. SB performed XPS measurement and analysis. OM and RZ performed ^{57}Fe Mössbauer and analysis. MH and PWM performed XAS measurement and analysis. ZM, RVJ, MB and RZ wrote the paper with the input and contribution of all authors. Open Access funding enabled and organized by Projekt DEAL.

Conflict of Interest

The authors declare no competing interests.

Data Availability Statement

The data that support the findings of this study are available in the supplementary material of this article.

Keywords: iron catalysis · single atoms · reductive amination · carbonyl compounds · amines

[1] H. Lehtimäki, L. Aarikka-Stenroos, A. Jokinen, P. Jokinen, *Routledge.* **2023**, (Verlag).
[2] J.-M. Valverde, C. Avilés-Palacios, *Sustainability.* **2021**, *13*, 12652–12667.
[3] S. V. Kruchten, F. V. Eijk, *Circular Economy SDGs.* **2020**.
[4] The World Needs Precious Metals and Rare Earth Elements. https://www.boldbusiness.com/ infrastructure/world-needs-precious-metals-rare-earth-elements/.
[5] How rare earth elements' hidden properties make modern technology possible. https://www. sciencenews.org/article/rare-earth-elements-properties-technology.
[6] S. Ivanova, M. M. Tejada, *Catalysts* **2020**, *10*, 247–249.
[7] M. Seehra, A. Bristow, *Noble and Precious Metals-Properties, Nanoscale Effects and Applications* **2018**.
[8] J. Hagen, *Wiley-VCH Verlag GmbH & Co. KgaA*, **2005**.
[9] F. Poovan, V. G. Chandrashekhar, K. Natte, R. V. Jagadeesh, *Catal. Sci. Technol.* **2022**, *12*, 6623–6649.
[10] J. Heveling, *J. Chem.* **2012**, *89*, 1530–1536.
[11] B. M. Weckhuysen, *Blackwell Verlag GmbH*, **2023**.
[12] A. Corma, *Angew. Chem. Int. Ed.* **2016**, *55*, 6112–6113.

[13] Global Catalyst Market Analysis, Share, Trends, Forecast. https://www.expertmarketresearch. com/reports/catalyst-market.
[14] E. de Santiago, et al., *Endoscopy.* **2022**, *54*, 797–826.
[15] Global carbon footprints in **2022**: https://www.iea.org/reports/CO_2-emissions-in-2022.
[16] UN sustainability goals: https://sdgs.un.org/goals.
[17] R. M. Bullock, J. G. Chen, L. Gagliardi, P. J. Chirik, O. K. Farha, C. H. Hendon, C. W. Jones, J. A. Keith, J. Klosin, S. D. Minteer, R. H. Morris, A. T. Radosevich, T. B. Rauchfuss, N. A. Strotman, A. Vojvodic, T. R. Ward, J. Y. Yang, Y. Surendranath, *Science* **2020**, *369*, eabc3183.
[18] D. Formenti, F. Ferretti, F. K. Scharnagl, M. Beller, *Chem. Rev.* **2018**, *119*, 2611–2680.
[19] R. Gebbink, M. Moret, *John Wiley & Sons*, **2019**.
[20] D. Wang, Astruc. D, *Chem. Soc. Rev.* **2017**, *46*, 816–854.
[21] Daily Metal Prices. https://www.dailymetalprice.com/.
[22] I. Bauer, H.-J. Knölker, *Chem. Rev.* **2015**, *115*, 3170–3387.
[23] A. Fürstner, *ACS Cent. Sci.* **2016**, *2*, 778–789.
[24] D. Wei, C. Darcel, *Chem. Rev.* **2019**, *119*, 2550–2610.
[25] B. Singh, M. B. Gawande, A. D. Kute, R. S. Varma, P. Fornasiero, P. McNeice, R. V. Jagadeesh, M. Beller, R. Zbořil, *Chem. Rev.* **2021**, *121*, 13620–13697.
[26] F. Haber, R. Rossignol, *Ind. Eng. Chem.* **1913**, *5*, 328–331.
[27] M. Appl, *Ammonia. Ullmann's Encyclopedia of Industrial Chemistry* **2006**, *153*.
[28] B. H. Davis, M. L. Occelli, *Fischer–Tropsch Synthesis, Catalysts, and Catalysis: Advances and Applications* **2016**.
[29] S. Abelló, D. Montané, *ChemSusChem* **2011**, *4*, 1538–1556.
[30] A. Q. Wang, J. Li, & T. Zhang, *Nat. Rev. Chem.* **2018**, *2*, 65–81.
[31] Z. Li, S. F. Ji, Y. W. Liu, X. Cao, S. B. Tian, Y. J. Chen, Z. Q. Niu, Y. D. Li, *Chem. Rev.* **2019**, *120*, 623–682.
[32] J. Li, M. F. Stephanopoulos, Y. N. Xia, *Chem. Rev.* **2020**, *120*, 11699–11702.
[33] L. C. Liu, A. Corma, *Chem. Rev.* **2018**, *118*, 4981–5079.
[34] X. Hai, Y. Zheng, Q. Yu, N. Guo, S. B. Xi, X. X. Zhao, S. Mitchell, X. H. Luo, V. Tulus, M. Wang, X. Y. Sheng, L. B. Ren, X. D. Long, J. Li, P. He, H. H. Lin, Y. G. Cui, X. N. Peng, J. W. Shi, J. Wu, C. Zhang, R. Q. Zou, G. G. -Gosálbez, J. P. -Ramírez, M. J. Koh, Y. Zhu, J. Li, J. Lu, *Nature* **2023**, *622*, 754–760.
[35] X. J. Cui, W. Li, P. Ryabchuk, K. Junge, M. Beller, *Nat. Catal.* **2018**, *1*, 385–397.
[36] W. G. Liu, L. L. Zhang, X. Liu, X. Y. Liu, X. F. Yang, S. Miao, W. T. Wang, A. Q. Wang, T. Zhang, *J. Am. Chem. Soc.* **2017**, *139*, 10790–10798.
[37] J. Gu, C.-S. Hsu, L. C. Bai, H. M. Chen, X. L. Hu, *Science* **2019**, *364*, 1091–1094.
[38] T. Marshall-Roth, N. J. Libretto, A. T. Wrobel, K. J. Anderton, M. L. Pegis, N. D. Ricke, T. V. Voorhis, J. T. Miller, Y. Surendranath, *Nat. Commun.* **2020**, *11*, 5283.
[39] K. K. Sun, H. B. Shan, H. Neumann, G.-P. Lu, M. Beller, *Nat. Commun.* **2022**, *13*, 1848.
[40] H. F. Qi, S. X. Mao, J. Rabeah, R. Y. Qu, N. Yang, Z. P. Chen, F. Bourriquen, J, Yang, J. F. Li, K. Junge, M. Beller, *Angew. Chem. Int. Ed.* **2023**, *62*, e2023119.
[41] R. V. Jagadeesh, A.-E. Surkus, H. Junge, M.-M. Pohl, J. Radnik, J. Rabeah, H. M. Huan, V. Schunemann, A. Bruckner, M. Beller, *Science* **2013**, *342*, 1073–1076.
[42] S. A. Lawrence, *Amines: Synthesis, Properties and Applications.* Cambridge University Press **2004**.
[43] A. Ricci, *Amino Group Chemistry: From Synthesis to the Life Sciences.* Wiley-VCH. **2008**.
[44] Top 200 brand name drugs by retail sales in **2022**. https://bpb-us-e2.wpmucdn.com/sites.arizona .edu/dist/9/130/files/2023/11/NjardarsonGroup2022Top200PosterV5.pdf.
[45] O. Afanasyev, E. Kuchuk, D. L. Usanov, D. Chusov, *Chem. Rev.* **2019**, *119*, 11857–11911.
[46] K. Murugesan, T. Senthamarai, V. G. Chandrashekhar, K. Natte, P. Kamer, M. Beller, R. V. Jagadeesh, *Chem. Soc. Rev.* **2020**, *49*, 6273–6328.
[47] T. Irrgang, R. Kempe, *Chem. Rev.* **2020**, *120*, 9583–9674.
[48] R. V. Jagadeesh, K. Murugesan, A. S. Alshammari, H. Neumann, M.-M. Pohl, J. Radnik, M. Beller, *Science* **2017**, *358*, 326–332.
[49] G. Hahn, P. Kunnas, N. D. Jonge, R. Kempe, *Nat. Catal.* **2019**, *2*, 71–77.
[50] T. Senthamarai, K. Murugesan, J. Schneidewind, N. V. Kalevaru, W. Baumann, H. Neumann, P. C. J. Kamer, M. Beller, R. V. Jagadeesh, *Nat Commun* **2018**, *9*, 4123–4135.
[51] X. Zhang, S. Q. Xu, Q. F. Li, G. L. Zhou, H. A. Xia, *RSC Adv.* **2021**, *11*, 27042–27058.
[52] M. Chatterjee, T. Ishizakaa, H. Kawanami, *Green Chem.* **2016**, *18*, 487–496.
[53] A. Dunbabin, F. Subrizi, J. M. Ward, T. D. Sheppard, H. C. Hailes, *Green Chem.* **2017**,*19*, 397–404.
[54] J. Han, X. Y. Meng, L. Lu, J. J. Bian, Z. P. Li, C. W. Sun, *Adv. Funct. Mater.* **2019**, *29*, 1808872.
[55] B. Matsoso, K. Ranganathanab, B. K. Mutumaab, T. Lerotholib, G. Jonescd, N. J. Coville, *RSC Adv.* **2016**, *6*, 106914–106920.
[56] F. Jaouen, J. Herranz, M. Lefevre, J.-P. Dodelet, U. I. Kramm, I. Herrmann, P. Bogdanoff, J. Maruyama, T. Nagaoka, A. Garsuch, J. R. Dahn, T. Olson, S. Pylypenko, P. Atanassov, E. A. Ustinov, *ACS Appl. Mater. Interfaces.* **2009**, *1*, 1623–1639.
[57] T. Yamashita, & P. Hayes, *Appl. Surf. Sci.* **2008**, *254*, 2441–2449.
[58] W. B. Qiu, N. Yang, D. Luo, J. Y. Wang, L. R. Zheng, Y. C. Zhu, E. M. Akinoglu, Q. M. Huang, L. L. Shui, R. M. Wang, G. F. Zhou, X. Wang, Z. W. Chen, *Appl. Catal. B.* **2021**, *293*, 120216.
[59] G. Filoti, M. D. Kuz'min, J. Bartolomé, *Phys. Rev. B.* **2006**, *74*, 134420.
[60] D. Nachtigallová, A. Antalík, R. Lo, R. Sedlák, D. Manna, J. Tuček, J. Ugolotti, L. Veis, Ö. Legeza, J. Pittner, R. Zbořil, P. Hobza, *Chem. Eur. J.* **2018**, *24*, 13413–13417.
[61] E. Barreiro, A. E. Kümmerle, C. A. M. Fraga, *Chem. Rev.* **2011**, *111*, 5215–5246.
[62] J. Chatterjee, F. Rechenmacher, H. Kessler, *Angew. Chem. Int. Ed.* **2013**, *52*, 254–269.
[63] H. T. Clarke, H. B. Gillespie, S. Z. Weisshaus, *J. Am. Chem. Soc.* **1933**, *55*, 4571–4687.

Manuscript received: April 25, 2024
Accepted manuscript online: June 24, 2024
Version of record online: August 7, 2024